Ca^{2+}- and Volume-sensitive Chloride Currents Are Differentially Regulated by Agonists and Store-operated Ca^{2+} Entry

Alexander Zholos,[1] Benjamin Beck,[1] Vadym Sydorenko,[1] Loïc Lemonnier,[1] Pascal Bordat,[2] Natalia Prevarskaya,[1] and Roman Skryma[1]

[1]Laboratoire de Physiologie Cellulaire, INSERM EMI 0228, Université des Sciences et Technologie de Lille, 59655 Villeneuve d'Ascq, France

[2]Centre de Recherche Pierre Fabre Dermo-Cosmétique, 31322 Castanet-Tolosan, France

ABSTRACT Using patch-clamp and calcium imaging techniques, we characterized the effects of ATP and histamine on human keratinocytes. In the HaCaT cell line, both receptor agonists induced a transient elevation of $[Ca^{2+}]_i$ in a Ca^{2+}-free medium followed by a secondary $[Ca^{2+}]_i$ rise upon Ca^{2+} readmission due to store-operated calcium entry (SOCE). In voltage-clamped cells, agonists activated two kinetically distinct currents, which showed differing voltage dependences and were identified as Ca^{2+}-activated ($I_{Cl(Ca)}$) and volume-regulated ($I_{Cl, swell}$) chloride currents. NPPB and DIDS more efficiently inhibited $I_{Cl(Ca)}$ and $I_{Cl, swell}$, respectively. Cell swelling caused by hypotonic solution invariably activated $I_{Cl, swell}$ while regulatory volume decrease occurred in intact cells, as was found in flow cytometry experiments. The PLC inhibitor U-73122 blocked both agonist- and cell swelling–induced $I_{Cl, swell}$, while its inactive analogue U-73343 had no effect. $I_{Cl(Ca)}$ could be activated by cytoplasmic calcium increase due to thapsigargin (TG)-induced SOCE as well as by buffering $[Ca^{2+}]_i$ in the pipette solution at 500 nM. In contrast, $I_{Cl, swell}$ could be directly activated by 1-oleoyl-2-acetyl-*sn*-glycerol (OAG), a cell-permeable DAG analogue, but neither by $InsP_3$ infusion nor by the cytoplasmic calcium increase. PKC also had no role in its regulation. Agonists, OAG, and cell swelling induced $I_{Cl, swell}$ in a nonadditive manner, suggesting their convergence on a common pathway. $I_{Cl, swell}$ and $I_{Cl(Ca)}$ showed only a limited overlap (i.e., simultaneous activation), although various maneuvers were able to induce these currents sequentially in the same cell. TG-induced SOCE strongly potentiated $I_{Cl(Ca)}$, but abolished $I_{Cl, swell}$, thereby providing a clue for this paradox. Thus, we have established for the first time using a keratinocyte model that $I_{Cl, swell}$ can be physiologically activated under isotonic conditions by receptors coupled to the phosphoinositide pathway. These results also suggest a novel function for SOCE, which can operate as a "selection" switch between closely localized channels.

KEY WORDS: human keratinocytes • histamine receptors • cell swelling • chloride channels • store-operated Ca^{2+} entry

INTRODUCTION

Epidermal keratinocytes form the major living (i.e., noncornified) part of the epidermis. It is becoming increasingly evident that the activity of various ion channels plays an essential, but not yet fully understood, role in their functions such as cell stratification and cornification (Mauro et al., 1993; Jones and Sharpe, 1994b; Wohlrab and Markwardt, 1999; Wohlrab et al., 2000; Koegel and Alzheimer, 2001). Among them, chloride channels play a role in membrane resting potential of human keratinocytes (Wohlrab et al., 2000) and in the responses to several physiological skin agonists (Koegel and Alzheimer, 2001). Moreover, both Ca^{2+}-activated ($I_{Cl(Ca)}$) and swelling-activated ($I_{Cl, swell}$) chloride currents are present in keratinocytes (Rugolo et al., 1992; Koegel and Alzheimer, 2001). The former has been implicated in the depolarizing response of keratinocytes to ATP, bradykinin, or histamine, while less is known about the properties, mechanisms of activation, and functional significance of the latter.

In other cell types, Cl^- channels show remarkably different biophysical and pharmacological properties and respond to a diverse array of gating stimuli (e.g., membrane potential change, rise in $[Ca^{2+}]_i$, cell swelling, binding of various signaling molecules, and ions) (for reviews see Jentsch et al., 2002; Nilius and Droogmans, 2003). Among these channels, volume-regulated anion channels (VRACs) are today attracting more and more scientific attention. Indeed, numerous cellular physiological processes, including hormonal action, proliferation,

N. Prevarskaya and R. Skryma share senior authorship.

Correspondence to Roman Skryma: phycel@pop.univ-lille1.fr

A. Zholos' present address is Laboratory of Molecular Pharmacology of Cellular Receptors and Ion Channels, Bogomoletz Institute of Physiology, 4 Bogomoletz Street, Kiev 01024, Ukraine.

Abbreviations used in this paper: HTS, hypotonic solution; NPPB, 5-nitro-2-(3-phenylpropylamino) benzoic acid; OAG, 1-oleoyl-2-acetyl-*sn*-glycerol; PMA, phorbol-12-myristate-13-acetate; RVD, regulatory volume decrease; SES, standard external solution; SOCE, store-operated calcium entry; SP, staurosporine; TG, thapsigargin; VRAC, volume-regulated anion channel.

J. Gen. Physiol. © The Rockefeller University Press • 0022-1295/2005/02/197/15 $8.00
Volume 125 February 2005 197–211
http://www.jgp.org/cgi/doi/10.1085/jgp.200409161

differentiation, and apoptosis (Lang et al., 2000) are associated with cell volume modulation, and the primary event during regulatory volume decrease seems to be the activation of VRACs. Despite the vast amount of experimental data about volume-regulated Cl^- channels that has been accumulated over the last few years, it is still not clear whether expression of these channels is a common feature of all cells or whether changes in their expression pattern reflect a special developmental and/or the functional state of cell. Furthermore, the mechanisms of activation and regulation of VRACs are not clearly understood and continue to appear rather contradictory (Nilius and Droogmans, 2003). A large variety of factors that modulate these channels have been proposed: G proteins, arachidonic acid and its metabolites, phosphorylation reactions involving Ca^{2+}/calmodulin-dependent protein kinase II, PKC, PKA, tyrosine kinase, cytoskeleton, and gene expression. However, as yet no ubiquitous modulating factor of volume-sensitive Cl^- channels themselves, or of their volume sensor, has been demonstrated. Volume-regulated Cl^- channels are undoubtedly of special interest in studies of keratinocytes because of their possible involvement in the process inducing the cell switch from a proliferating to a nonproliferating, differentiated state, as was shown in other cell types (Nilius et al., 1996). However, very little is known either about the mechanisms of their activation and regulation in keratinocytes, or even about regulatory mechanisms and properties of other types of chloride channels, especially of calcium-regulated channels.

Thus, in the present study, we aimed to investigate whole-cell Cl^- currents in human keratinocytes under conditions of $[Ca^{2+}]_i$ "clamped" at either a resting level (e.g., 100 nM) or an elevated level of 500 nM. We specifically aimed to investigate whether Ca^{2+}-activated Cl^- current $I_{Cl(Ca)}$ and swelling-activated Cl^- current $I_{Cl, swell}$, which are present in keratinocytes (demonstrated by Rugolo et al., 1992 and Koegel and Alzheimer, 2001), can be evoked, or modulated, by receptor agonists and capacitative Ca^{2+} entry. Therefore, we examined the effects on these currents of ATP and histamine, since keratinocytes are typically exposed to these substances during skin injury, inflammatory skin diseases, and allergic reactions. The action of these two receptor agonists is of physiological importance as HaCaT cells express H_2 histamine and P2Y2 purinergic receptors coupled to a phosphoinositide pathway (Pillai and Bikle, 1992; Koizumi and Ohkawara, 1999; Koegel and Alzheimer, 2001).

Moreover, we have previously shown, in another cell line, that store-operated calcium entry (SOCE) following ER calcium store depletion can specifically inhibit VRAC. Thus, our second aim was to extend these findings and to investigate whether similar mechanisms of VRAC regulation are present in keratinocytes.

The results of our experiments on an immortalized, nontumor cell line (HaCaT) of human keratinocytes show that ATP and histamine could activate two types of channels, which were identified as calcium-activated chloride channel (CLCA, $I_{Cl(Ca)}$) and volume-regulated anion channel (VRAC, $I_{Cl, swell}$) according to their biophysical characteristics and pharmacological properties. $I_{Cl(Ca)}$ was activated via the well-established mechanism of Ca^{2+} mobilization through $InsP_3$ receptors and SOCE, while $I_{Cl, swell}$ apart from its common induction by hypotonic solution could be activated by diacylglycerols in a PKC-independent manner without the involvement of $InsP_3$. Moreover, cell swelling caused by hypotonic solution invariably activated $I_{Cl, swell}$, while regulatory volume decrease occurred in intact cells as we measured in flow cytometry experiments.

Intriguingly, these two different chloride currents could be activated in the same cell sequentially, but rarely simultaneously, to produce any significantly overlapping currents. Attempting to understand this phenomenon, we turned our attention to a possible SOCE-dependent modulation of chloride channels (Lemonnier et al., 2002a; Abeele et al., 2003). SOCE occurred in HaCaT cells in response to both agonists and thapsigargin (TG) treatment. It abolished $I_{Cl, swell}$ but strongly potentiated $I_{Cl(Ca)}$, providing an explanation for the above paradox. These findings suggest a novel mechanism according to which cells can translate a graded Ca^{2+} entry via SOC channels into different ion channel responses.

MATERIALS AND METHODS

Cell Culture

HaCaT keratinocytes (provided by CNRS UNR 5543) were cultured in Dulbecco's modified Eagle's medium (DMEM; GIBCO BRL) containing 5 mM glutamax, a thermostable analogue of glutamine, and supplemented with 10% FBS (Seromed; Poly-Labo). The culture medium also contained 10 mg/l kanamycine. Cells were routinely grown in 50-ml flasks (Poly-Labo) and kept at 37°C in a humidified incubator in an air/CO_2 (95/5%) atmosphere. For electrophysiology, the cells were subcultured in Petri dishes (Nunc) and used within 3–6 d.

Calcium Imaging

Cells were plated onto glass coverslips and loaded with 4 μM Fura-2 a.m. at room temperature for 45 min in HBSS containing (in mM) 140 NaCl, 5 KCl, 2 $MgCl_2$, 2 $CaCl_2$, 0.3 Na_2HPO_3, 0.4 KH_2PO_4, 4 $NaHCO_3$, 5 glucose, and 10 HEPES adjusted to pH 7.4 with NaOH. The coverslips were then placed in a perfusion chamber on the stage of the microscope. Fluorescence images of the cells were recorded with a video image analysis system (Quanticell). The Fura-2 fluorescence, at an emission wavelength of 510 nm, was recorded by exciting the probe alternatively at 340 and 380 nm. The signal ratio at 340/380 nm was converted into $[Ca^{2+}]_i$ level using an in vitro calibration. All reagents soluble in water, ethanol, or dimethyl sulfoxide were diluted to their final concentration in HBSS and applied using a perfusion system. For each type of experiment, data were accumulated from at least three measurements.

Flow Cytometry

Cell volume changes were measured using a FACScalibur flow cytometer (Becton Dickinson) and "Q Cell Quest" software for data analysis (Bratosin et al., 1997). The light-scatter channels were set on linear gains. Cells in suspension in normal or hypo-TEA solutions were gated for forward-angle scatters and 5,000 particles of each gated population were analyzed. Cells were passed in a single-file through a laser beam by continuous flow of a fine stream of the suspension. Each cell scatters some of the laser light and that way, the cytometer typically measures several parameters simultaneously for each cell. These include flow angle forward scatter intensity, which is proportional to the cell diameter.

Patch-clamp Recordings and Data Analysis

For electrophysiological recordings, HaCaT cells were separated by a brief trypsin treatment and plated in small volume (500 μl) dishes, which were placed on the stage of an inverted microscope. The culture medium was replaced with standard external solution (SES) before establishing whole-cell configuration. Patch pipettes were made of borosilicate glass (resistance 3–5 MΩ). Membrane current was recorded at room temperature with either the voltage-clamp amplifier, Axopatch 200B using a Digidata 1200 interface and pClamp software (Axon Instruments Inc.), or a HEKA EPC-8 amplifier (HEKA Elektronik). Series resistance was compensated by 70–80%. Recordings were sampled at 1–4 kHz and stored on a hard disk.

Cells were held at a holding potential of −40 mV, which is close to their average resting potential (Koegel and Alzheimer, 2001). Voltage ramps from −100 to 100 mV (200 or 400 ms duration) were applied at 10-s intervals to monitor current amplitudes continuously. For precise measurements of the steady-state currents at different test potentials and evaluation of the voltage-dependent kinetics of the currents, we employed a voltage-step protocol, which consisted of a 1–2.8-s pulses to test potentials ranging from −120 to 100 mV applied every 5–20 s with an increment of 10 or 20 mV. Tail currents were measured using a standard double-pulse protocol, as shown in Fig. 2 B. Capacitance currents were removed for the clarity of the illustrations.

The Ag/AgCl bath reference electrode was connected using a 3 M KCl bridge in order to minimize changes of liquid junction potentials, which occur with external solutions of various ion compositions. The offset potential between pipette solution and SES was zeroed before the formation of a seal (typically several GOhm). Using an open pipette and performing the most significant changes of the external solution ion composition (e.g., replacing 140 mM NaCl with 140 mM CsCl or reducing Cl^- concentration by 120 mM), we measured changes of the junction potential in the range of 0.5–1.8 mV. Thus, the membrane potentials were not corrected for these small values.

Data were analyzed and plotted using the pClamp 6 (Axon Instruments Inc.) and MicroCal Origin software (MicroCal Software, Inc.). Values are given as the mean ± SEM. The Student's *t* test was used for statistical comparison, and differences were judged to be statistically significant when $P < 0.05$.

Solutions

The standard external solution consisted of (in mM) 140 NaCl; 0.5 $CaCl_2$; 2 $MgCl_2$; 10 HEPES and 10 glucose; pH adjusted to 7.3 with NaOH. The Cs^+-rich external solution was prepared by replacing 140 mM NaCl with 140 mM CsCl; pH was adjusted to 7.3 with CsOH. In low-Cl^- external solution, 120 mM CsCl was replaced with an equimolar amount of caesium methanesulfonate. The osmolarity of all external isotonic solutions was adjusted to 320 mosmol/l by the addition of D-mannitol. The composition of hypotonic solution (HTS) (200 mosmol/l) was 90 TEA-Cl; 5 glucose; 10 HEPES; 0.5 $CaCl_2$; 2 $MgCl_2$; pH adjusted to 7.3 with TEA-OH. TEA ions do not interfere with VRAC channels, but help to eliminate possible interference from K^+ and other cation channels (Shuba et al., 2000). We also verified that a similar swelling-sensitive current was invariably activated in HaCaT cells in response to a simple SES dilution (e.g., 150–300 μl of distilled water added directly to the bath).

Pipettes were filled with the following solution (in mM): CsCl 40, BAPTA 10, CsOH 40; Cs-methanesulfonate 60; $MgCl_2$ 1; K_2ATP 1; Na_2GTP 0.1; HEPES 5; pH adjusted to 7.2 with CsOH. Either 4.6 or 7.1 mM $CaCl_2$ was added to the pipette solution in order to buffer free Ca^{2+} to 100 or 500 nM, respectively (calculated using EqCal software, Biosoft). When $[Ca^{2+}]_i$ was clamped at 500 nM, it is specifically indicated in the text and figure legends. The osmolarity of all internal solutions was adjusted to 305 mosmol/l by D-mannitol. External but not internal BAPTA inhibits VRACs (Lemonnier et al., 2002b). In tests using EGTA instead of BAPTA ($n = 9$), no differences in $I_{Cl,\ swell}$ generation were found.

Thus, the solutions were designed to facilitate the recording of Cl^- currents at fixed $[Ca^{2+}]_i$ to avoid changes in any intracellular Ca^{2+}-dependent processes. Importantly, strong $[Ca^{2+}]_i$ buffering in the bulk cytoplasm is an established methodology to reveal "cross-talk" between SOC and VRAC channels in subplasmalemmal microdomains (Lemonnier et al., 2002a). The use of Cs^+ effectively abolishes K^+ currents, as K^+ channels have a low permeability to this cation. The extracellular Ca^{2+} concentration was 0.5 mM in order to reduce Ca^{2+} influx, unless this was desirable, in which case it was raised to 5 or 10 mM as stated.

All chemicals were from Sigma-Aldrich. Necessary supplements were added directly to the respective solutions, in concentrations that could not significantly change the osmolarity. Changes in the external solutions were performed using a multibarrel puffing micropipette with common outflow that was positioned in close proximity to the cell under investigation. During the experiment, the cell was continuously superfused with the solution via the puffing pipette to reduce possible artifacts related to the switch from static to moving solution and vice versa. Complete external solution exchange was achieved in <1 s.

RESULTS

General Appearances and Modes of Activation of Two Distinct Chloride Currents in HaCaT Cells

Patch-clamp experiments were performed on 97 HaCaT cells that had a mean membrane capacitance of 39 ± 8 pF. In keratinocytes clamped using a 100 nM Ca^{2+} pipette, solution membrane currents were small and time independent, suggesting their background conductance origin (Fig. 1, Ba, Ca, and Da).

Recently it has been shown that in HaCaT cells that express H_2 histamine and P2Y2 purinergic receptors, agonists of these G protein/PLC-coupled receptors produce complex changes in the membrane potential, consisting of an initial transient depolarization, followed by a more sustained hyperpolarization (Koegel and Alzheimer, 2001). However, the underlying ion currents have not been characterized, although pharmacological evidence has suggested that the depolarization was predominantly mediated by a 4,4'-diisothio-

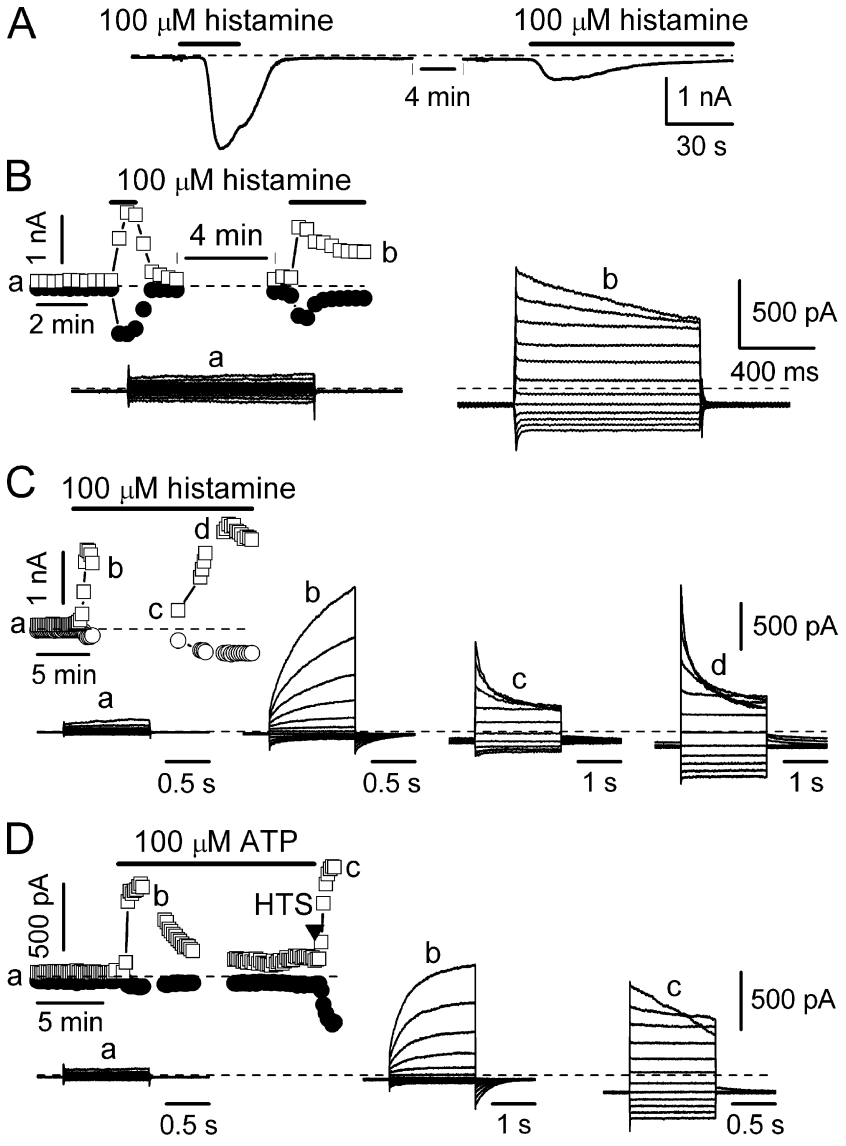

FIGURE 1. Histamine, ATP, and cell swelling activate two different currents in HaCaT cells. (A) Histamine-induced membrane current responses in a HaCaT cell measured at the holding potential of −60 mV. Ca^{2+} concentration in the pipette solution in this experiment, as well as those illustrated in B–D, was buffered at 100 nM. In this and all subsequent figures, drug administration period and zero current level are indicated by solid and dotted horizontal lines, respectively. (B) Histamine application evoked current that, upon a voltage step, showed rapid activation and characteristic inactivation at potentials positive to 40 mV. Current amplitude is shown at two different potentials. In this and all subsequent figures, open squares denote current amplitude at 100 mV and closed circles at −100 mV. Current amplitude was monitored by applying voltage ramps from −100 to 100 mV from a holding potential of −40 mV. Superimposed current traces measured by voltage step protocol during the gaps labeled a and b are shown below. (C) In a different cell, using similar voltage step protocol, 100 μM histamine initially evoked current, which was distinct from that illustrated in B. It was characterized by slow activation during depolarizing voltage steps, complete absence of inactivation even at strong depolarization, and by a much smaller inward component (traces labeled b measured during the respective gap in the time course plot). However, in the continuous presence of histamine, this current disappeared, or at least it was greatly diminished, while current response similar to that shown in B appeared (traces labeled c and d). (D) Two distinct Cl^- currents were differentially activated by ATP and cell swelling in the same HaCaT cell. ATP application evoked a transient current that developed within 2.5 min and nearly completely decayed in ~10 min in the continuous presence of ATP. Reducing tonicity of the external solution from 320 to 200 mosmol/l evoked a large sustained current. Superimposed current traces were evoked by voltage steps from −40 mV to different levels ranging from −120 to 100 mV during the periods indicated by the corresponding letters in the time course plot. HTS-induced current was stable during the next 30 min of recording (not depicted).

cyanato-stilbene-2,2'-disulfonic acid (DIDS)– and niflumic acid–sensitive Cl^- current, consistent with the expression of two types of Ca^{2+}-activated Cl^- channels. In contrast, hSK4 K^+ channel activity mediated membrane hyperpolarization.

Histamine applied at 100 μM evoked a large inward current at −60 mV, which was reversible upon agonist withdrawal and showed marked desensitization (Fig. 1 A). Voltage step protocol revealed a current with rapid activation/deactivation kinetics, which (within the limitations of the frequency response) could be described as instantaneous (Fig. 1 B). This current also showed a characteristic inactivation during voltage steps to potentials positive to 40 mV (Fig. 1 Bb). 9 out of 24 cells showed this type of current response. However, in another eight cells, an entirely different response initially occurred as shown in Fig. 1 C, whereas the remaining seven cells produced no measurable response to histamine application. The response of the second type was composed of instantaneous and time-dependent current components, which were observed during voltage steps. The latter component was particularly pronounced at depolarized potentials, resulting in a prominent outwardly rectifying current–voltage relationship (Fig. 2 A), while current of the first type showed a lesser degree of outward rectification (Fig. 2 C). Strikingly, in continuous agonist presence, response of the second type could eventually give way to the response of the first type (Fig.

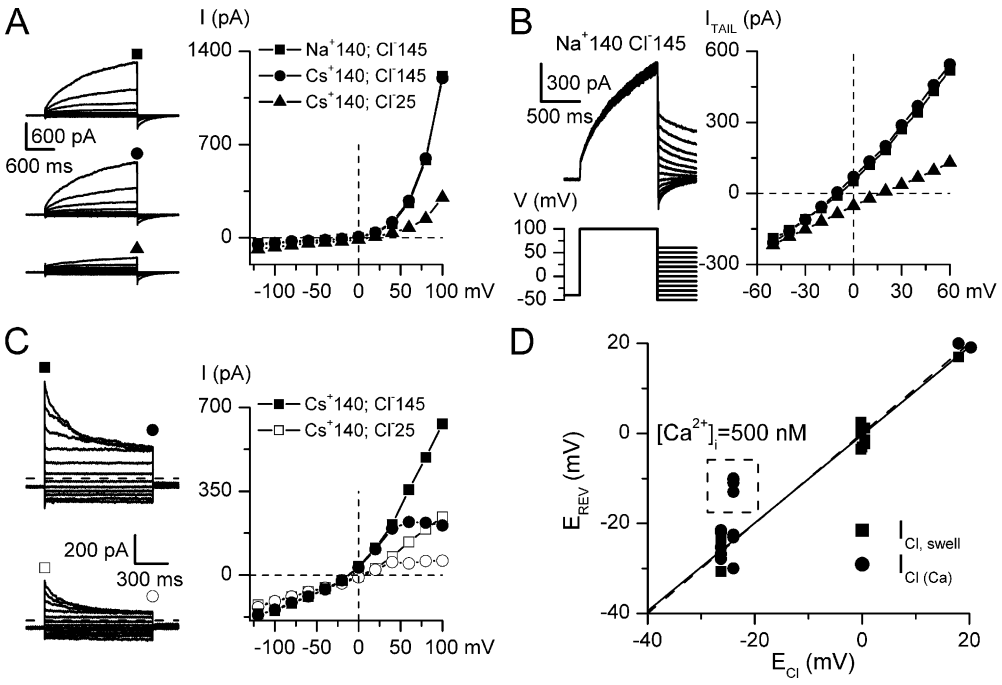

FIGURE 2. Ion nature of currents in HaCaT cells. (A) Slow outwardly rectifying current that was persistently activated by $[Ca^{2+}]_i$ elevated to 500 nM (clamped using 10 mM BAPTA) and recorded in external solutions of different ion composition as indicated. Left, superimposed current traces; right, corresponding I–V relationships. Current amplitudes were measured at the end of the test voltage step. (B) Tail current analysis of the current in the same cell. Left, an example of current traces and the voltage protocol used to measure tail currents. Tail current amplitude was obtained by exponential approximation of the tail current to the onset of the negative voltage step. Right, amplitude of the tail current plotted vs. test potential under the same ion conditions as in A and shown by the corresponding symbols. (C) 100 μM histamine applications evoked current with properties characteristic of $I_{Cl,\ swell}$. Replacing the external solution of 140 mM Cs^+ with 140 mM Na^+ had no effect on this current (not depicted), whereas reducing external Cl^- concentration from 145 to 25 mM markedly reduced the amplitude of the outward current and shifted the reversal potential of the current positively. Superimposed current traces measured by applying voltage steps from −40 mV to test potentials ranging from −120 to 100 mV under different ion conditions are shown on the left. Right panel shows I–V relationships measured as shown by the corresponding symbols for ion conditions indicated at the top. In this experiment, $[Ca^{2+}]_i$ was clamped at 100 nM. (D) Summary of the reversal potential measurements in 14 cells displaying $I_{Cl,\ swell}$ and 13 cells displaying $I_{Cl(Ca)}$ under variable electrochemical gradients for chloride ions. Note that in four cells clamped using pipette solution with 500 nM Ca^{2+} (data points inside the dotted box) E_{REV} was 11–14 mV more positive compared with E_{Cl}, which could indicate the presence of Ca^{2+}-dependent cationic channels in some HaCaT cells. The dotted line is drawn for complete correspondence of E_{Cl} and E_{REV}. The solid line shows linear regression analysis of the data points excluding those inside the box.

1 C), showing that channels of both types were present in the same cell but were not activated simultaneously, at least to an appreciable degree. It was thus unlikely that differing channel expression patterns determined the agonist response type. Responses of the first and second type also commonly occurred during the action of ATP (3 and 4, respectively, out of 12 cells tested as shown in Fig. 1 D; 5 cells were nonresponsive). By a number of criteria, current of the second type was identified as Ca^{2+}-activated chloride current, $I_{Cl(Ca)}$ (see below).

Most cells recover from cell swelling by increasing membrane permeability to ions, such as K^+ and Cl^-, which results in the regulatory volume decrease (RVD) through the loss of intracellular ions and water. This is associated with the opening of VRACs, which have been well characterized in many cell types but not as yet in keratinocytes. The above-described current response of the first type to histamine (Fig. 1 Bb) had a phenotype characteristic of the $I_{Cl,\ swell}$ currents carried via VRACs in other cells (Voets et al., 1997; Lang et al., 1998; Shuba et al., 2000; for reviews see Jentsch et al., 2002; Nilius and Droogmans, 2003). Thus, we further checked that $I_{Cl,\ swell}$ can be activated by HTS in HaCaT cells. In intact HaCaT cells, RVD developed following HTS application (e.g., Fig. 6 C, light columns), and this phenomenon could be inhibited by addition of 5-nitro-2-(3-phenylpropylamino) benzoic acid (NPPB) to the solution, implying the involvement of Cl^- channels (not depicted). In voltage-clamp cells, we verified visually that the application of HTS induced cell swelling that was accompanied by a slow development of a current with properties typical of $I_{Cl,\ swell}$ (Fig. 1 D). This current was very similar in its voltage dependence and activation/deactivation kinetics to the above-described response to histamine of the first type (e.g., Fig. 1 B).

$I_{Cl,\ swell}$ developed invariably in all cells studied (n = 27), even in those that responded to agonists with the $I_{Cl(Ca)}$ type (Fig. 1 D), again arguing that both Cl^- channel types were expressed in the same cell. It was sustained as long as the cell was kept in HTS (i.e., up to at least several tens of minutes), but declined to the background level with the time constant of 53 ± 10 s (n = 7) following the restoration of the external solution tonicity (e.g., Fig. 6 A).

Two types of agonist-induced currents could be clearly distinguished based on their distinct pheno-

type, yet a possibility of some overlap between them needed further clarification. A prominent inward tail current was associated with $I_{Cl(Ca)}$ (Fig. 1, C and D; Fig. 2, A and B; Fig. 3, A and C; Fig. 4 B; Fig. 7 C), but it was absent in case of $I_{Cl, swell}$ (Fig. 1, B–D; Fig. 2 C; Fig. 3 A; Fig. 4 A; Fig. 6 B; Fig. 7 C). Thus, any significant $I_{Cl(Ca)}$ appeared to be absent when $I_{Cl, swell}$ developed. In the case of $I_{Cl(Ca)}$, the instantaneous component could arguably be due to $I_{Cl, swell}$ contribution, and inactivation of the latter at positive potentials could be masked by slow activation of $I_{Cl(Ca)}$ during voltage steps. However, it should be noted that the two components are typically recorded in $I_{Cl(Ca)}$ current in other cell types (e.g., Greenwood et al., 2001). The instantaneous current reflects Ca^{2+}-activated Cl^- conductance at the holding potential. Thus, this component can be seen to occur upon a sudden change in the chloride electrochemical gradient when voltage jumps to a new level. Consistent with this interpretation, we found that (a) the instantaneous component during $I_{Cl(Ca)}$ occurrence showed a perfect ohmic dependence on test potential unlike the instantaneous component of $I_{Cl, swell}$, which showed some degree of outward rectification (e.g., Fig. 2 C, data for $I_{Cl(Ca)}$ not depicted); and (b) there was deactivation of $I_{Cl(Ca)}$ at negative potentials, i.e., during a negative voltage step, current increased instantaneously, but declined to a smaller steady-state level (e.g., Fig. 1 Cb). In contrast, $I_{Cl, swell}$ did not show any deactivation at negative potentials (e.g., Fig. 1 Dc), and thus only a small nondeactivating component of $I_{Cl(Ca)}$ could be potentially attributed to $I_{Cl, swell}$. If this were indeed $I_{Cl, swell}$ and taking into account its voltage dependence (e.g., $I_{Cl, swell}$ at 100 mV was on average 2.2 ± 0.3 times larger than current at −120 mV, $n = 15$), one can estimate that at 100 mV, $I_{Cl, swell}$ could contribute only 14 ± 2% to the whole-cell current ($n = 14$) when the dominant current was $I_{Cl(Ca)}$. Moreover, our pharmacological data suggest hardly any overlap between these currents since NPPB efficiently blocked $I_{Cl(Ca)}$ and any contaminating $I_{Cl, swell}$ would be revealed, but was not observed in the presence of NPPB (see Fig. 4 Ba).

The activation kinetics of $I_{Cl(Ca)}$ was voltage independent, as it had been previously described in other cell types (e.g., Kuruma and Hartzell, 2000; Greenwood et al., 2001). In 10 cells, the time constant was 387 ± 33 ms at 20 mV, nonsignificantly increasing to 479 ± 78 ms at 100 mV ($P = 0.29$). To minimize the cell-to-cell variability, the time constant at 100 mV was normalized as 1.0, and then the values at 20, 40, 60, and 80 mV were, respectively, 1.07 ± 0.09, 0.98 ± 0.08, 1.04 ± 0.06, and 1.01 ± 0.05. Deactivation of this current upon a negative voltage step was only weakly voltage dependent. It remained the same at negative potentials (e.g., 173 ± 11 ms at −50 mV and 166 ± 67 ms at −10 mV), increasing about twofold at positive potentials (e.g., 290 ± 26 ms at 10 mV and 343 ± 47 ms at 60 mV) ($n = 4$). There was also a much smaller inward current associated with this conductance compared with $I_{Cl, swell}$.

Chloride Dependency

An outwardly rectifying current in HaCaT cells was carried by Cl^- as was evident from the following: (a) replacing external Na^+ with Cs^+ had no effect, but lowering the Cl^- concentration in the external solution induces a significant reduction in the outward current, alongside a positive shift of its reversal potential (Fig. 2 A); and (b) close match between its tail current reversal potential and E_{Cl} in ion substitution experiments (Fig. 2 B). Also, the slope conductance strongly decreased in low-Cl^- solution (c.f. compare triangles to circles or to squares in Fig. 2 B, right).

Similar observations were made for $I_{Cl, swell}$ where the outward current was also significantly reduced and its reversal potential shifted positively when $[Cl^-]_o$ was reduced from 140 to 25 mM (Fig. 2 C). Fig. 2 D summarizes the above reversal potential measurements for $I_{Cl, swell}$ (squares, $n = 19$) and $I_{Cl(Ca)}$ (circles, $n = 17$) in different cells and with different electrochemical chloride gradients. The dotted line is drawn for the case where $E_{REV} = E_{Cl}$. On average, there was a very close match between the measured and theoretical values. The correlation analysis gave $R = 0.99$ with $P < 0.0001$ (continuous line in Fig. 2 D).

Mechanisms of $I_{Cl(Ca)}$ Activation by Receptor Stimulation: SOCE and $[Ca^{2+}]_i$ Elevation

The underlying mechanisms of chloride channel activation by receptor agonists are potentially very complex, since G protein–coupled receptors produce diverse signals. However, since both H_2 and P2Y2 receptors converge to activate a common phosphoinositide cascade thus releasing and emptying Ca^{2+} stores, in the next series of experiments we explored the role of SOCE in $I_{Cl(Ca)}$ activation as one plausible common factor brought about by H_2 or P2Y2 receptor activation.

The importance of testing this Ca^{2+} entry pathway is highlighted by the following controversy. On the one hand, $I_{Cl(Ca)}$ was induced directly by raising $[Ca^{2+}]_i$ to 500 nM alone without receptor activation ($n = 14$), and the current remained very stable when $[Ca^{2+}]_i$ was strongly buffered at 500 nM (Fig. 3 A, I–V relationships and traces shown in the top inset). On the other hand, a similar current developed at 100 nM $[Ca^{2+}]_i$ when agonists were applied (Fig. 1, C and D). A question then arises as to how Ca^{2+} released from the store, if this were an exclusive source of Ca^{2+} for channel activation, could induce channel activity in the presence of a high-capacity exogenous Ca^{2+} buffer in the pipette solution.

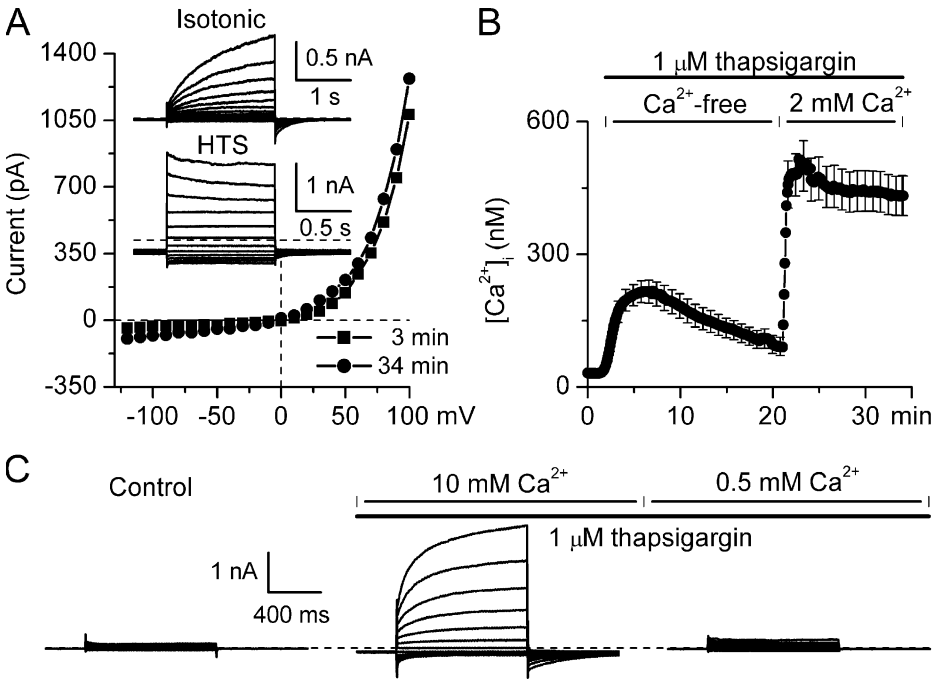

FIGURE 3. $I_{Cl(Ca)}$ is persistently active at $[Ca^{2+}]_i$ = 500 nM and facilitated by capacitative Ca^{2+} entry. (A) Sustained activation of $I_{Cl(Ca)}$ under conditions of elevated intracellular Ca^{2+} concentration ($[Ca^{2+}]_i$ was clamped at 500 nM). Shortly after breakthrough (3 min), $I_{Cl(Ca)}$ activation was revealed by applying voltage step protocol (superimposed traces in the inset). The activation was persistent (compare two I–V relationships for the current amplitude at the end of the pulse measured at 3 and 34 min after the beginning of the experiment). The inset shows superimposed current traces measured in isotonic solution (top) and, in the same cell, $I_{Cl,\ swell}$ traces recorded during HTS application (bottom). (B) Ca^{2+} imaging experiments revealed TG-induced SOCE in HaCaT cells. Each data point represents mean value of the $[Ca^{2+}]_i$ signal in 120 cells. Note that the SEM values are shown for every 10th data point for clarity. (C) Superimposed current traces recorded in the same HaCaT cell with $[Ca^{2+}]_i$ buffered at 100 nM in control (left), after treatment of the cell for 8 min with 1 μM thapsigargin, followed by the addition of 10 mM Ca^{2+} to the external solution (middle) and 10 min after reducing external Ca^{2+} to 0.5 mM (right).

This paradox could be resolved on the assumption that it was additionally a steady Ca^{2+} influx due to Ca^{2+} store depletion that activated $I_{Cl,Ca}$. Notably, when the bulk cytosolic Ca^{2+} concentration was fixed at 500 nM, the cells also responded to HTS by generating large currents through VRACs (e.g., the bottom set of traces in Fig. 3 A, inset).

To reveal whether SOCE was present in HaCaT cells, we used fluorometric $[Ca^{2+}]_i$ measurements and found that cells responded to TG treatment (which depletes Ca^{2+} stores by inhibiting SERCA-dependent Ca^{2+} reuptake) by an elevation of $[Ca^{2+}]_i$ in a Ca^{2+}-free solution followed by a more sustained $[Ca^{2+}]_i$ rise when external Ca^{2+} was readmitted (Fig. 3 B). This is a classical sequence of events that is interpreted as a Ca^{2+} store release signal (due to passive Ca^{2+} leak from the ER), followed by a SOCE signal. Similar observations were made when histamine or ATP were applied to release Ca^{2+} from the store (Fig. 7 A).

We next tested if $I_{Cl(Ca)}$ could be induced using a similar protocol. Fig. 3 C illustrates an experiment whereby $[Ca^{2+}]_i$ was buffered at 100 nM and background current was therefore small. Treatment with TG followed by external Ca^{2+} rise to 10 mM resulted in a strong $I_{Cl(Ca)}$ response. However, when the external Ca^{2+} concentration was reduced back to 0.5 mM, this current disappeared almost completely. Similar observations were made on eight cells exposed either to 5 or 10 mM external Ca^{2+} following TG treatment. Since activation of $I_{Cl(Ca)}$ was seen despite the bulk $[Ca^{2+}]_i$ being strongly buffered at 100 nM, these results imply a close relation between Ca^{2+} entry channels and Ca^{2+}-activated Cl^- channels, such that Ca^{2+} entering the cell could activate the latter channels before being bound to BAPTA deeper in the cytosol.

Differences in the Pharmacological Properties of $I_{Cl(Ca)}$ and $I_{Cl,\ swell}$

In other cell types, many drugs have been reported to block $I_{Cl,\ swell}$ and $I_{Cl(Ca)}$ with substantial variations in their potency. However, NPPB and DIDS are the two most common blockers of $I_{Cl,\ swell}$ and $I_{Cl(Ca)}$ (Jentsch et al., 2002; Nilius and Droogmans, 2003). $I_{Cl,\ swell}$ is typically blocked by NPPB and DIDS with the IC_{50} values in the range of 5–100 μM. However, in HaCaT cells, NPPB was not as potent as DIDS (Fig. 4 A). $I_{Cl(Ca)}$ in most cells is inhibited more potently by NPPB (IC_{50} 5–100 μM) than by DIDS (IC_{50} 0.1–2 mM). This was also the case in HaCaT cells, as illustrated in Fig. 4 B. NPPB at 100 μM almost abolished $I_{Cl(Ca)}$ (Fig. 4 B, a and b) while DIDS at the same concentration was less effective (Fig. 4 Bc). All these inhibitory effects were reversible after the drug was removed. These pharmacological differences in the sensitivity to NPPB and DIDS further highlight distinction between the two chloride currents in human keratinocytes.

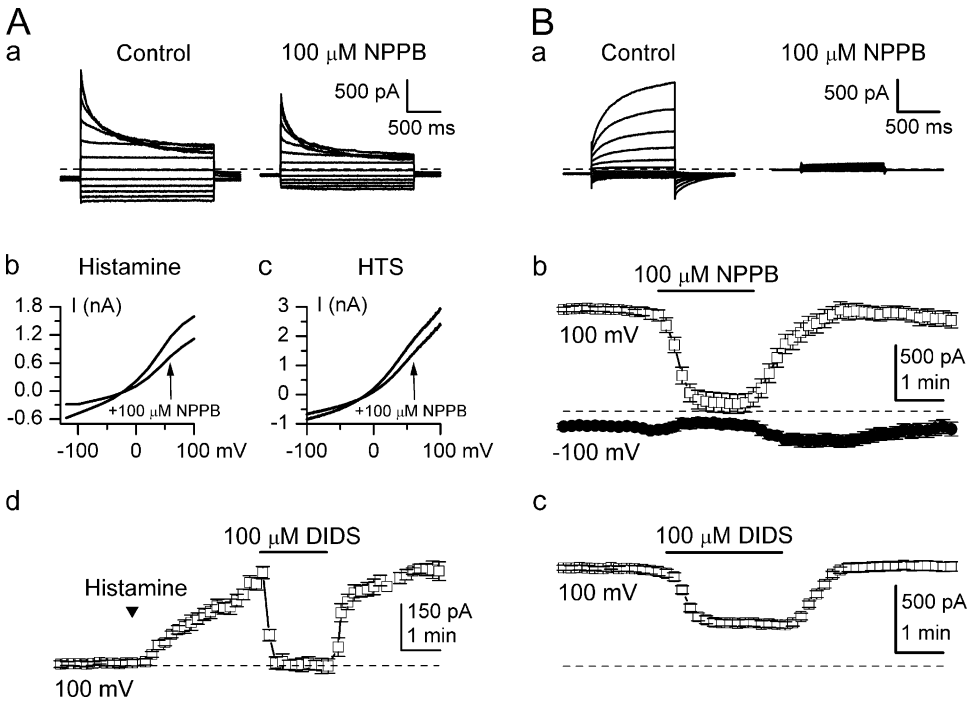

FIGURE 4. Blocking action of NPPB and DIDS on Cl^- currents in HaCaT cells. (Aa) Superimposed current traces induced by the action of histamine (100 μM) measured before and after NPPB application. (A, b and c) I–V relationships of $I_{Cl,\ swell}$ induced by 100 μM histamine application (b) or HTS of 200 mosmol/l (c) before and after 100 μM NPPB application (the latter are indicated by the arrows). (Ad) Mean histamine-induced $I_{Cl,\ swell}$ amplitude was measured at 100 mV while DIDS at 100 μM was applied as shown by the horizontal bar (n = 4). These experiments were performed with $[Ca^{2+}]_I$ = 100 nM. (Ba) Superimposed current traces of $I_{Cl(Ca)}$ induced by high-Ca^{2+} pipette solution ($[Ca^{2+}]_i$ = 500 nM) measured before and after 100 μM NPPB application. (B, b and c) $I_{Cl(Ca)}$ amplitude was monitored by a ramp protocol while NPPB (b) or DIDS (c) was applied at 100 μM as shown by the horizontal bars (n = 4 for both drugs). Note that current amplitudes are steady from the beginning of measurements as high-Ca^{2+} pipette solution evokes a sustained $I_{Cl(Ca)}$ (compare with Fig. 3 A).

Mechanisms of $I_{Cl,\ swell}$ Activation by Receptor Stimulation: the Involvement of the PLC/DAG Pathway and No Role for PKC

Our observations that $I_{Cl,\ swell}$ could be activated under isotonic conditions by histamine or ATP strongly imply its biological importance in HaCaT cells. Moreover, we found that these chloride channels could also be constitutively active (unpublished data) as previously shown for VRACs (Duan et al., 1997; Greenwood and Large, 1998). It is now emerging that channels carrying $I_{Cl,\ swell}$ in other cell types can be modulated through receptor activation (e.g., α- and β-adrenoceptors, as recently shown by Ellershaw et al., 2002, differentially modulate $I_{Cl,\ swell}$ in rabbit portal vein myocytes). However, the fact that $I_{Cl,\ swell}$ can be induced by a G protein–coupled receptor activation in isotonic environment (e.g., Fig. 1, A and B) is a novel observation.

Since $I_{Cl,\ swell}$, although not being activated by intracellular calcium, was inhibited by SOCE (see below), we further studied the mechanism by which the PLC-mediated agonist's signal transduction could stimulate $I_{Cl,\ swell}$. The PLC blocker U-73122 inhibited agonist-induced $I_{Cl,\ swell}$ while U-73343, its inactive analogue, at the same concentration had no effect. Compared with portal vein myocytes (Ellershaw et al., 2002), the inhibition at the same concentration of 1 μM was stronger (i.e., 72 ± 14%, n = 5). U-73122 was found to retain its inhibitory effect on HTS-induced $I_{Cl,\ swell}$ (Fig. 5 A; inhibition by 75 ± 4% at 1 μM, n = 3). This observation was consistent with the recent suggestion that tonic PLC activity was relevant to the activation of $I_{Cl,\ swell}$ in rabbit portal vein myocytes (Ellershaw et al., 2002).

Moreover, $I_{Cl,\ swell}$ was directly activated by 1-oleoyl-2-acetyl-*sn*-glycerol (OAG), a synthetic membrane-permeable analogue of DAG, which is the major intermediate second messenger generated by the PLC activation (Fig. 5 B). Investigations in the same experimental conditions into whether OAG was able to activate $I_{Cl(Ca)}$ gave a negative result (unpublished data). PKC is the major downstream DAG effector enzyme and has also been suggested as one of the molecular linkages between changes in cell volume and $I_{Cl,\ swell}$ generation (Duan et al., 1997; 1999; Zhong et al., 2002). The authors have suggested that this mechanism involves the dephosphorylation of PKC-phosphorylated sites on the channel protein. Thus, we tested the action of staurosporine (SP), a PKC inhibitor, on OAG-activated $I_{Cl,\ swell}$, but found no effect (Fig. 5 B). Furthermore, the phorbol ester phorbol-12-myristate-13-acetate (PMA), which directly stimulates PKC, had no effect on the basal current or $I_{Cl,\ swell}$ induced by HTS (Fig. 5 C), suggesting that PKC played no role in $I_{Cl,\ swell}$ generation or modulation in HaCaT cells.

Interestingly, when the current was activated by a 100 μM OAG application, 100 μM ATP failed to produce any additional effect on $I_{Cl,\ swell}$ (Fig. 5 B), although a reverse sequence of application showed some increase in $I_{Cl,\ swell}$. These results imply that DAG may be the sole

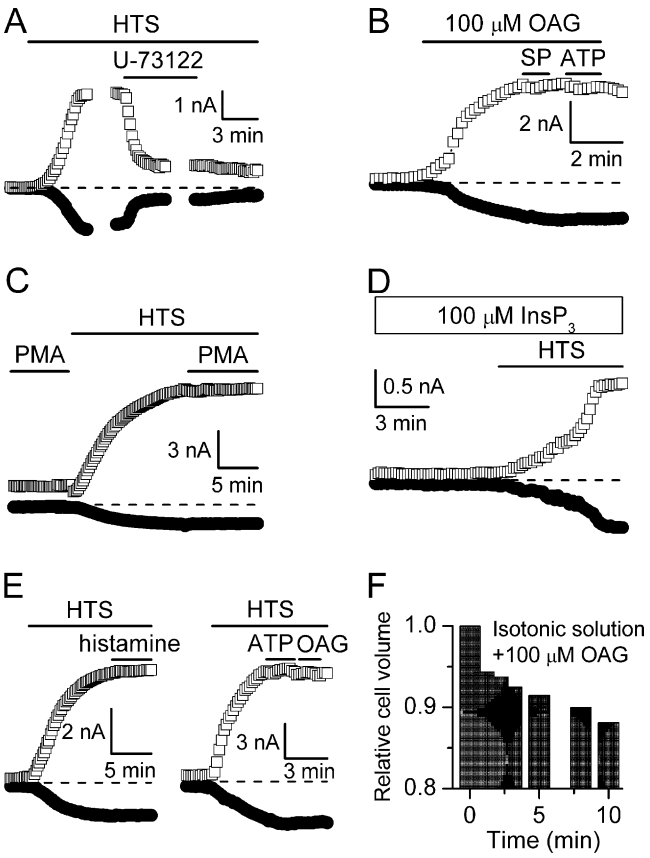

FIGURE 5. PLC and OAG-dependent, PKC-independent activation of $I_{Cl,\ swell}$ in HaCaT cells. (A) HTS-induced $I_{Cl,\ swell}$ was strongly inhibited by 1 μM U-73122 application. Current–voltage relationships were measured by the voltage step protocol during the gaps (not depicted). (B) OAG (100 μM) application induced $I_{Cl,\ swell}$ in HaCaT cells, which was not affected by the PKC inhibitor staurosporine (SP, 1 μM) or ATP application (100 μM). (C) $I_{Cl,\ swell}$ current response to HTS (200 mosmol/l) during the application of phorbol-12-myristate-13-acetate (PMA, 100 nM, $n = 10$). Note that preceding PMA application had no noticeable effect on the membrane current. (D) $InsP_3$ included in the pipette solution did not induce $I_{Cl,\ swell}$ or prevent its occurrence in response to HTS ($n = 5$). Note, however, that the response to HTS during $InsP_3$ infusion via the pipette was of a much smaller amplitude compared with controls (e.g., A–C and E, note different current scale). (E) HTS-induced (200 mosmol/l) $I_{Cl,\ swell}$ was not affected by histamine (100 μM), ATP (100 μM), or OAG (100 μM) applications ($n = 4$). (F) Flow cytometry measurements showed cell volume decrease under isotonic conditions starting 30 s after 100 μM OAG application. Each column represents relative cell volume of 8,000 keratinocytes. OAG was applied at time zero. In the experiments illustrated in A–E, $[Ca^{2+}]_i$ was buffered at 100 nM.

intermediate in evoking $I_{Cl,\ swell}$ during the action of agonists on HaCaT cells, at least when DAG concentration is high. Consistent with this hypothesis, we found that when another important messenger generated during PLC activation, $InsP_3$, was included in the pipette solution (even at a high concentration of 100 μM), it failed to induce $I_{Cl,\ swell}$ on its own and did not prevent an HTS response (c.f. findings reported by Ellershaw et al., 2002). SP under these conditions was also ineffective. However, it was notable that in the presence of $InsP_3$, the current developed reluctantly and reached only a fraction of its normal size (Fig. 5 D, note different amplitude scale compared with A, B, C, and E without $InsP_3$). This suggested inhibition rather than potentiation of $I_{Cl,\ swell}$ during the action of $InsP_3$, a significant observation that deserved further attention in light of our recent findings in LNCaP cells (Lemonnier et al., 2002a). Finally, we verified that both agonists and OAG became ineffective in inducing any additional current when $I_{Cl,\ swell}$ fully developed in response to HTS application (Fig. 5 E).

Taken together, these results suggest that in HaCaT cells, histamine and ATP induce $I_{Cl,\ swell}$ via PLC activation, through a DAG-dependent $InsP_3$-independent pathway, without the involvement of PKC-dependent phosphorylation. Since these effects are not cumulative with those produced by cell swelling (Fig. 5 E), convergence on a common pathway seems very likely. It should be mentioned, however, that HTS-induced $I_{Cl,\ swell}$ compared with agonist-induced $I_{Cl,\ swell}$ was larger (at 100 mV 3.85 ± 0.66 nA, $n = 15$ vs. 1.31 ± 0.46 nA, $n = 12$; $P = 0.006$), although cell-to-cell variations were significant in both cases. The former also showed a slower rate and a lesser degree of inactivation at positive potentials (compare Fig. 1 D, Fig. 6 B, and Fig. 7 C to Fig. 1 C, Fig. 2 C, Fig. 4 A, and Fig. 7 C, but note slow inactivation in Fig. 1 B).

In flow cytometry experiments, we observed ~12% reduction in the cell volume in response to 100 μM OAG application under isotonic conditions (Fig. 5 F), an effect that could well be related to $I_{Cl,\ swell}$ activation with a subsequent loss of chloride ions and water. It can thus be hypothesized that, assuming a putative "volume sensor" is indeed a part of VRAC, this down-regulates agonist-induced (since cells shrink), but up-regulates swelling-induced channel activity, while in both cases, DAG is a primarily signaling molecule.

$I_{Cl,\ swell}$ Inhibition by Store-operated Ca^{2+} Entry

In contrast to $I_{Cl(Ca)}$, SOCE had the opposite effect on $I_{Cl,\ swell}$, as shown in Fig. 6 A. Control experiments showed that without TG treatment, there was a small increase in the osmotically activated $I_{Cl,\ swell}$ amplitude when Ca^{2+} concentration in the external solution was raised to 10 mM (traces on the left). This small potentiation might not be related to the effect of the external Ca^{2+}, as the same effect was observed when 15 mM NaCl was added to the external solution. In both cases, the tonicity increased equivalently to $[Cl^-]_o$ rises, thus accounting for a larger outward current.

In TG-treated cells, however, strong inhibition of HTS-induced $I_{Cl,\ swell}$ was observed at elevated external Ca^{2+} concentration (Fig. 6 A, traces on the right). Su-

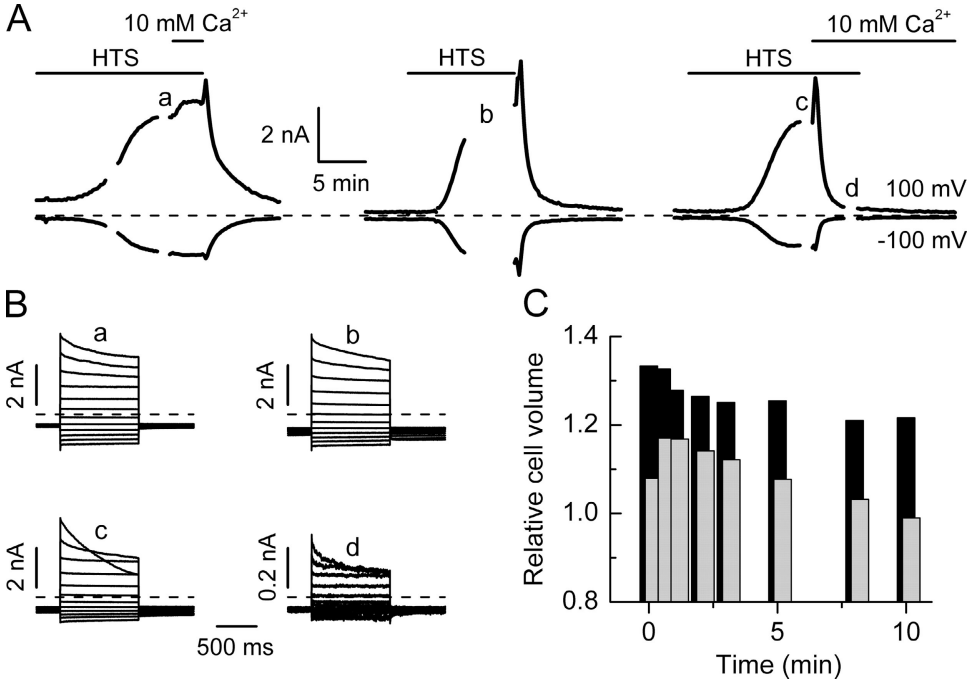

FIGURE 6. SOCE-dependent inhibition of $I_{Cl,\ swell}$. (A) Under control conditions (no thapsigargin treatment), the outward $I_{Cl,\ swell}$ induced by HTS somewhat increased upon 10 mM external $CaCl_2$ application (traces on the left). However, in a 1 μM thapsigargin-treated cell, HTS-induced $I_{Cl,\ swell}$ was nearly abolished by external Ca^{2+} elevation to 10 mM (traces on the right). Note that there was some transient increase in the outward current, which preceded the inhibition, probably due to an increase in the external chloride concentration as seen in control cells as well. $[Ca^{2+}]_i$ was buffered at 100 nM. (B) Superimposed current traces measured by applying voltage steps ranging from −120 to 100 mV with a 20-mV increment during the gaps denoted by the same letters in A. (C) Flow cytometry measurements showed cell RVD in response to HTS (applied at time zero) in control (light columns). However, 1 μM TG-treated keratinocytes (dark columns) remained swollen even 15 min after HTS application (133% of the initial volume). Each column represents relative cell volume of 8,000 keratinocytes.

perimposed current traces recorded during periods marked a–d are shown in panel B.

Thus, these experiments directly confirmed $I_{Cl,\ swell}$ inhibition by SOCE, consistently with the above-described effects of $InsP_3$. In flow cytometry experiments, we observed a strong reduction of RVD in TG-treated keratinocytes (Fig. 6 C) and a similar effect was produced by DIDS or NPPB (not depicted). Notably, the initial cell swelling was also more pronounced in TG-treated cells (Fig. 6 C).

Since buffering $[Ca^{2+}]_i$ to 500 nM using 10 mM BAPTA/7.1 mM $CaCl_2$ mixture did not interfere with $I_{Cl,\ swell}$ generation (e.g., Fig. 3 A) and mean current amplitudes were similar both at 100 and 500 nM $[Ca^{2+}]_i$ (at 100 mV 3.85 ± 0.66 nA, $n = 15$ vs. 3.58 ± 0.79 nA, $n = 7$, respectively; $P > 0.8$), an efficient current inhibition by SOCE implies that VRACs are poorly accessible to the exogenous intracellular Ca^{2+} buffer but directly accessible to SOCE. Thus, the interaction between VRACs and SOCE can likely occur in the microdomains from the inner side of the membrane with VRACs in a juxtaposition to SOC channels (Fig. 8; compare with our recent findings in human prostate cancer epithelial cells; Lemonnier et al., 2002a). Furthermore, since $I_{Cl(Ca)}$ was activated by the agonists and SOCE (Fig. 1, C and D; Fig. 3 C) despite Ca^{2+} concentration in the cytosol was "clamped" at 100 nM, colocalization of Ca^{2+}-dependent chloride channels with SOC channels also seems very likely.

Hypothesis of SOCE as the Main "Switch" Mechanism Favoring the Activation of Either $I_{Cl,\ swell}$ or $I_{Cl(Ca)}$

Our results indicated a clear differential role of SOCE in the regulation of $I_{Cl,\ swell}$ and $I_{Cl(Ca)}$. Thus, we further tested the hypothesis that the magnitude of SOCE is the major factor determining the type of the response. Fig. 7 A shows that both histamine and ATP activated SOCE in HaCaT cells in a manner similar to TG (compare with Fig. 3 B). A mechanistic explanation of the paradoxical observation is illustrated in Fig. 7 B, showing that the cell was able to switch from the predominant $I_{Cl(Ca)}$ mode into the predominant $I_{Cl,\ swell}$ mode (Fig. 1 C) and vice versa (Fig. 7 C) while only a limited overlap between these currents had occurred. Our model is based on just one assumption: SOCE inhibits VRAC current more readily than it activates $I_{Cl(Ca)}$. This could be due to intrinsic differences in the Ca^{2+} sensitivity of the respective channels, but a possibility not to be ignored is a closer proximity of VRAC to the SOC channel (Fig. 8, note the difference in the channel juxtaposition). Indeed, in LNCaP cells, VRAC channels were found to be completely inaccessible to bulk $[Ca^{2+}]_i$ (Lemonnier et al., 2002a), whereas in HaCaT cells, $[Ca^{2+}]_i$ at 500 nM readily induced $I_{Cl(Ca)}$ (Fig. 3 A), suggesting a greater exposure of the latter channel to global changes in $[Ca^{2+}]_i$. Thus, Ca^{2+} entering via SOCs may inhibit VRACs more efficiently by raising local $[Ca^{2+}]_i$ in the vicinity of VRACs, while a more distant $[Ca^{2+}]_i$ rise may be required to activate Ca^{2+}-

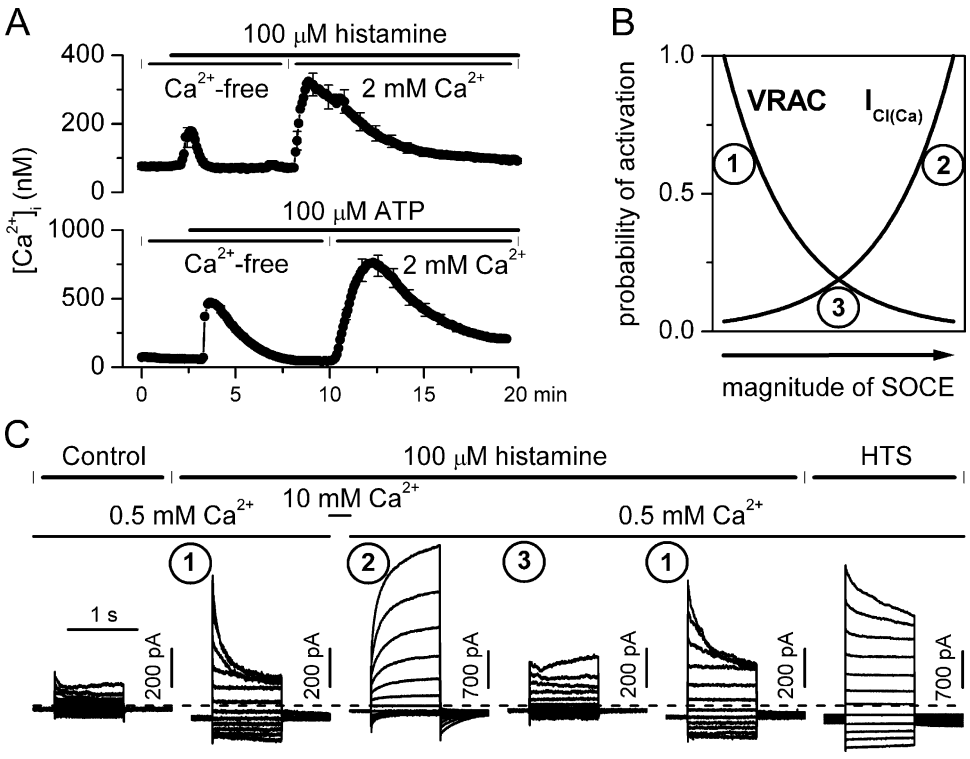

FIGURE 7. SOCE as a switch mechanism favoring activation of either $I_{Cl,\ swell}$ or $I_{Cl(Ca)}$ due to their differential control. (A) Ca^{2+} imaging experiments showed SOCE activation by 100 μM histamine (top) or 100 μM ATP application (bottom) in HaCaT cells. Each data point represents mean value of the $[Ca^{2+}]_i$ signal in 120 cells. Note that the SEM values are shown for every 10th data point. (B) Assuming differences in Ca^{2+} sensitivity or relative channel position, low magnitude SOCE favors $I_{Cl,\ swell}$ (mode 1), while high magnitude SOCE, by inhibiting $I_{Cl,\ swell}$ and potentiating $I_{Cl(Ca)}$, favors $I_{Cl(Ca)}$ (mode 2). At an intermediate magnitude SOCE, $I_{Cl,\ swell}$ is already inhibited while $I_{Cl(Ca)}$ is not yet fully activated, thus both currents are small (mode 3). (C) In a cell showing an initial $I_{Cl,\ swell}$ response to 100 μM histamine (1), $[Ca^{2+}]_{out}$ elevation from 0.5 to 10 mM resulted in a transition to $I_{Cl(Ca)}$ mode (2) but after $[Ca^{2+}]_{out}$ was returned to 0.5 mM, both currents were reduced (3) followed by an increase of $I_{Cl,\ swell}$ (1), presumably due to the removal of the Ca^{2+}-dependent inactivation of VRACs. Traces on the right were recorded in the same cell after its exposure to HTS. Note that $I_{Cl(Ca)}$ and HTS-induced $I_{Cl,\ swell}$ were plotted on a different current scale as they were larger in size. $[Ca^{2+}]_i$ was buffered at 100 nM.

dependent Cl^- channels. Given such postulated differences in the Ca^{2+} sensitivity and/or preferential access of SOCE to VRAC, it then follows that at relatively small SOCE, $I_{Cl,\ swell}$ will be a dominant current (mode 1), while relatively large SOCE will favor $I_{Cl(Ca)}$ activation (mode 2). The above postulated differences predict almost no response at an intermediate SOCE level (mode 3), which is a prerequisite of the model to explain the slight overlap experimentally observed between these different chloride currents.

As one most straightforward test of the suggested mechanism, we raised $[Ca^{2+}]_{out}$ from 0.5 to 10 mM when the cell responded to histamine by generating $I_{Cl,\ swell}$-type response (Fig. 7 C). Then, just before applying voltage steps, $[Ca^{2+}]_{out}$ was returned to 0.5 mM (in order to exclude any possible direct action of external Ca^{2+}). Following such an intervention, a large $I_{Cl(Ca)}$ developed but eventually declined before giving way to an $I_{Cl,\ swell}$ response, the latter being comparable to the initial response (Fig. 7 C). This sequence of response types was similar to the one seen during receptor desensitization at constant $[Ca^{2+}]_{out}$ (Fig. 1 C). It would consequently appear that both experiments can be commonly explained by the model in Fig. 7 B. We also verified that the cell was responsive to HTS (last set of traces in Fig. 7 C).

DISCUSSION

The results described in this report provide evidence for the differential activation by ATP and histamine of two distinct chloride currents, Ca^{2+}-activated, $I_{Cl(Ca)}$, and volume-sensitive, $I_{Cl,\ swell}$.

Recently, it has been shown that in keratinocytes, membrane permeability to K^+ and Cl^- is the major determinant of the resting potential (Wohlrab et al., 2000). Cl^- channels were also implicated as important targets for the action of various agonists on these cells. In another recent report, it was shown that opening of Ca^{2+}-activated Cl^- channels following receptor stimulation or "uncaged" $InsP_3$-induced Ca^{2+} release causes membrane depolarization due to Cl^- efflux in HaCaT cells (Koegel and Alzheimer, 2001). Also, in other cells, such currents via VRACs are directly relevant to cell growth, proliferation, and differentiation (Lang et al., 1998; Shen et al., 2000). Thus, in keratinocytes, Cl^- channels are of a significant biological importance.

Single chloride channel properties have been investigated, and several channel types were found with unitary conductance ranging from 16 to 200 pS (Galietta et al., 1991; Kansen et al., 1992; Mauro et al., 1993; Wohlrab et al., 2000), but the relation between these

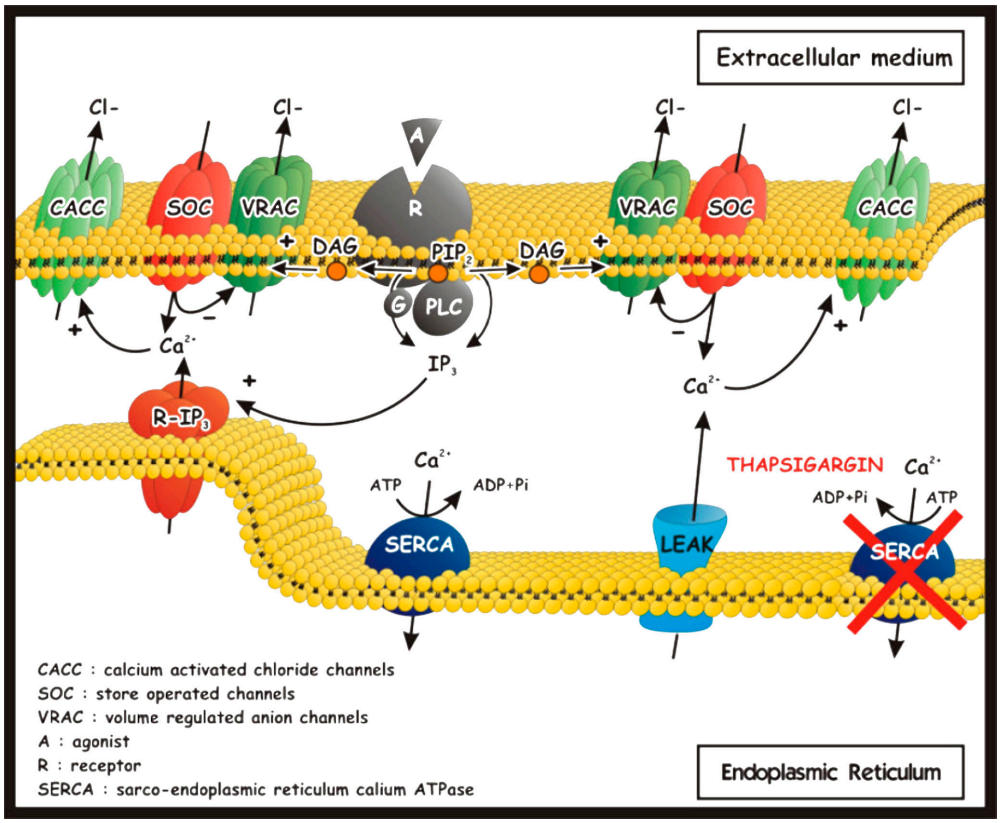

FIGURE 8. Agonists (A) activating PLC-coupled receptors (R), such as P2Y2 or H_2 receptors, stimulate production of $InsP_3$ and DAG. Initially DAG activates VRACs and the RVD phenomenon. Parallel $InsP_3$ production induces calcium store depletion and SOCE. The latter elevates subplasmalemmal calcium concentration. When it is low, VRACs are preferentially activated (denoted as mode 1 in Fig. 7 B). However, when the calcium concentration in the microdomain becomes high enough, VRACs are inhibited in spite of the continuing DAG production, and Ca^{2+}-dependent chloride channels are preferentially activated instead. TG, by inhibiting calcium uptake by SERCA proteins, evokes calcium store depletion via leak channels and thus induces SOCE. Therefore, it leads to the inhibition of VRACs and activation of $I_{Cl(Ca)}$ as $InsP_3$ does under physiological conditions. This scheme could explain how the two different chloride channels are regulated by calcium influx and why respective currents show only a limited degree of an overlap.

single channel events and macroscopic currents of HaCaT cells remains obscure.

Previous studies have shown specific regulation of chloride channels by the phosphoinositide pathway and SOCE (Ellershaw et al., 2002; Lemonnier et al., 2002a). Several studies have shown that receptor agonists, thapsigargin and $InsP_3$, induce Ca^{2+} release in keratinocytes (Pillai and Bikle, 1992; Rosenbach et al., 1993; Jones and Sharpe, 1994a,b; Biro et al., 1998; Koegel and Alzheimer, 2001). Associated capacitative calcium influx via store-operated Ca^{2+} channels has also been recently demonstrated in human keratinocytes (Gonczi et al., 2002). Therefore, keratinocytes, like other nonexcitable cells, are using SOCE as a major Ca^{2+} entry mechanism. H_2 histamine and P2Y2 purinergic receptors expressed in HaCaT are coupled to the phosphoinositide pathway (Koegel and Alzheimer, 2001). Stimulation of these receptors also activates a chloride current that was not characterized so far, although Ca^{2+}-activated Cl^- channels have been implicated in the depolarizing agonist-induced responses. Therefore, it was one of our primary aims to study this current and its link to calcium metabolism.

$I_{Cl(Ca)}$ properties in keratinocytes (i.e., voltage dependence, kinetics, blocking action of NPPB, and DIDS) are very similar to those of other cell types, particularly if a parallel is made with studies where $I_{Cl(Ca)}$ was evoked by pipette solution containing clamped $[Ca^{2+}]_i$ (Ishikawa and Cook, 1993; Arreola et al., 1996; Nilius et al., 1997; Greenwood et al., 2001; Britton et al., 2002; Piper et al., 2002). This allows direct comparison between different cell types, as any reliance on endogenous Ca^{2+} regulatory mechanisms in inducing $I_{Cl(Ca)}$ is removed or greatly diminished. Chloride selectivity (Fig. 2, A, B, and D), the blocking action of NPPB and DIDS (Fig. 4 B), persistent activation at 500 nM $[Ca^{2+}]_i$ (Fig. 3 A), and activation in a Ca^{2+}-dependent manner by SOCE (Fig. 3 C), taken together, strongly suggest that the first current activated by histamine or ATP can be identified as a Ca^{2+}-dependent Cl^- current as it has been recently suggested by Koegel and Alzheimer (2001). At variance with our observations on weakly voltage-dependent deactivation kinetics of this current

in HaCaT cells, Kuruma and Hartzell (2000) showed that the kinetics of Ca^{2+}-activated Cl^- current in *Xenopus* oocytes was strongly voltage dependent at low $[Ca^{2+}]_i$. However, the voltage sensitivity became less at submicromolar $[Ca^{2+}]_i$. Although it becomes evident that different types of Ca^{2+}-activated Cl^- channels exist, there is a possibility that weak voltage dependence of $I_{Cl(Ca)}$ deactivation in keratinocytes was also due to high local Ca^{2+} concentration during agonist-induced SOCE.

The other major agonist-induced current with instantaneous activation and deactivation kinetics and inactivation during voltage steps to positive potentials was also a chloride current (Fig. 2, C and D) sensitive to both DIDS and NPPB (Fig. 4 A). We have identified it as a volume-regulated Cl^- current, $I_{Cl,\ swell}$, since a similar current was induced by osmotic gradients (Fig. 1 D; Fig. 3 A; Fig. 6 B). The expression of VRAC agreed with our flow cytometry experiments showing RVD phenomenon in hypotonic solution (Fig. 6 C). Furthermore, RVD was inhibited when NPPB was added to the HTS, implying the involvement of Cl^- channels in this phenomenon (unpublished data). The biophysical and pharmacological properties of the $I_{Cl,\ swell}$ in HaCaT cells are very similar to those in other cells (Arreola et al., 1995; Boese et al., 1996; Voets et al., 1998; Shuba et al., 2000; Nilius et al., 2001; Ellershaw et al., 2002).

Concerning the pathways involved in the activation of both channel types, SOCE and the associated cytoplasmic calcium concentration increase can sufficiently explain the activation of $I_{Cl(Ca)}$ in HaCaT cells during G protein–coupled receptor activation (compare Fig. 1, C and D; Fig. 3, A and C; Fig. 8). The mechanisms of $I_{Cl,\ swell}$ activation are, however, more complex. Numerous intracellular pathways, second messengers, and kinases have been implicated in this process in other cell types. These currently include ATP, F-actin cytoskeleton, caveolins, tyrosine kinase, Rho and Rho-associated kinase, phosphatidylinositol 3-kinase, PKC, PKA, myosin light chain kinase, and Ca^{2+}/calmodulin-dependent protein kinase. Thus, there is a general agreement that several different, complex, and interacting intracellular events are likely to link cell volume changes to the generation and modulation of $I_{Cl,\ swell}$, and also that their relative contribution differs greatly according to cell type. Lastly, it is also possible that there is substantial diversity in the molecular identity of VRACs in different preparations.

Our present results show that in HaCaT keratinocytes, agonists induce $I_{Cl,\ swell}$ via PLC activation through a DAG-dependent $InsP_3$-independent pathway without the involvement of PKC-dependent phosphorylation (Figs. 5 and 8). The observations on the lack of PKC-dependent modulation are quite unique as there is growing awareness that $I_{Cl,\ swell}$ currents can be discriminated by their sensitivity to PKC modulators and anti–CLC-3 antibodies (Duan et al., 1999; Ellershaw et al., 2002; Yamamoto-Mizuma et al., 2004), but the current in HaCaT cells was neither up- nor down-regulated by PMA. It appears that the presence of CLC-3 mediates PKC-dependent regulation of $I_{Cl,\ swell}$ (Yamamoto-Mizuma et al., 2004); thus, this putative component of VRACs in other cell types might be lacking in keratinocytes.

Moreover, substantial convergence of the PLC/DAG system and cell swelling on a common pathway seems very likely. These results are in general agreement with the first report of the role of PLC in $I_{Cl,\ swell}$ activation in portal vein myocytes (Ellershaw et al., 2002). The analogy to the recently discovered gating of unrelated cation channels by DAG (e.g., TRPC3, Venkatachalam et al., 2003) is also quite remarkable. It remains to be established whether DAG itself mediates the activation of $I_{Cl,\ swell}$ via PLC activation in HaCaT cells. The products of DAG lipase (monoacylglycerol and arachidonic acid), as well as DAG kinase (phosphatidic acid) could be intermediate molecules, and the fact that OAG-induced current develops slowly (Fig. 5 B) is probably hinting in this direction. For TRP channels, the importance of other lipid second messengers is now better established (for recent review see Hardie, 2003). Also, it was found earlier that arachidonic acid could activate VRAC channels in endothelial cells (Nilius et al., 1994).

It was intriguing to observe that although both chloride conductances resided in the same cell, only one was predominantly active at a time (e.g., Fig. 1, C and D; Fig. 7 C). Interestingly, similar results were obtained in rat parotid acinar cells, where hypotonic solution and ionomycin, respectively, activated $I_{Cl,\ swell}$ and $I_{Cl(Ca)}$ of similar amplitudes (Arreola et al., 1995). One major novel finding in the present work is that $I_{Cl(Ca)}$ and $I_{Cl,\ swell}$ are differentially regulated by capacitative Ca^{2+} influx induced by TG treatment (Fig. 3 C; Fig. 6 A).

Based on these results, we propose a model that mechanistically explains the above paradox (Fig. 7 B). What could be the functional significance of such opposite effects? In HaCaT cells, SOCE is a major mechanism of $[Ca^{2+}]_i$ elevation, and this latter is known to induce their differentiation. $I_{Cl(Ca)}$ can provide negative feedback control to reduce Ca^{2+} influx via a store-operated pathway, since $I_{Cl(Ca)}$ will depolarize the membrane and thereby reduce the driving force for SOCE. In contrast, in cells with a smaller SOCE, $I_{Cl,\ swell}$ is a dominant response. Since this current is further inhibited by SOCE, membrane depolarization would be even less resulting in a larger capacitative Ca^{2+} entry. Thus, by modulating two different chloride conductances, SOCE can regulate its own magnitude through feedback effects on the membrane potential and hence electrochemical gradient for calcium ions.

These findings are consistent and further extend our previous observations. They imply that not only VRACs (as in LNCaP cells, Lemonnier et al., 2002a) but also Ca^{2+}-activated Cl^- channels might colocalize with SOC channels in cellular microdomains, which are directly accessible to SOC-mediated "Ca^{2+} channelling." Thus, it would now appear to be a more widely spread factor that significantly enhances both the selectivity and efficiency of this receptor-triggered Ca^{2+} entry pathway in modulating plasma membrane ion channel activities.

This work was supported by grants from INSERM and Ministère de l'Education Nationale. A. Zholos was supported by Region Nord Pas de Calais.

Olaf S. Andersen served as editor.

Submitted: 2 August 2004
Accepted: 17 December 2004

REFERENCES

Abeele, F.V., Y. Shuba, M. Roudbaraki, L. Lemonnier, K. Vanoverberghe, P. Mariot, R. Skryma, and N. Prevarskaya. 2003. Store-operated Ca^{2+} channels in prostate cancer epithelial cells: function, regulation, and role in carcinogenesis. *Cell Calcium.* 33:357–373.

Arreola, J., J.E. Melvin, and T. Begenisich. 1995. Volume-activated chloride channels in rat parotid acinar cells. *J. Physiol.* 484:677–687.

Arreola, J., J.E. Melvin, and T. Begenisich. 1996. Activation of calcium-dependent chloride channels in rat parotid acinar cells. *J. Gen. Physiol.* 108:35–47.

Biro, T., I. Szabo, L. Kovacs, J. Hunyadi, and L. Csernoch. 1998. Distinct subpopulations in HaCaT cells as revealed by the characteristics of intracellular calcium release induced by phosphoinositide-coupled agonists. *Arch. Dermatol. Res.* 290:270–276.

Boese, S.H., R.K. Kinne, and F. Wehner. 1996. Single-channel properties of swelling-activated anion conductance in rat inner medullary collecting duct cells. *Am. J. Physiol.* 271:F1224–F1233.

Bratosin, D., J. Mazurier, C. Slomianny, D. Aminoff, and J. Montreuil. 1997. Molecular mechanisms of erythrophagocytosis: flow cytometric quantitation of in vitro erythrocyte phagocytosis by macrophages. *Cytometry.* 30:269–274.

Britton, F.C., S. Ohya, B. Horowitz, and I.A. Greenwood. 2002. Comparison of the properties of CLCA1 generated currents and $I_{Cl(Ca)}$ in murine portal vein smooth muscle cells. *J. Physiol.* 539: 107–117.

Duan, D., C. Winter, S. Cowley, J.R. Hume, and B. Horowitz. 1997. Molecular identification of a volume-regulated chloride channel. *Nature.* 390:417–421.

Duan, D., S. Cowley, B. Horowitz, and J.R. Hume. 1999. A serine residue in ClC-3 links phosphorylation-dephosphorylation to chloride channel regulation by cell volume. *J. Gen. Physiol.* 113: 57–70.

Ellershaw, D.C., I.A. Greenwood, and W.A. Large. 2002. Modulation of volume-sensitive chloride current by noradrenaline in rabbit portal vein myocytes. *J. Physiol.* 542:537–547.

Galietta, L.J., V. Barone, M. De Luca, and G. Romeo. 1991. Characterization of chloride and cation channels in cultured human keratinocytes. *Pflugers Arch.* 418:18–25.

Gonczi, M., H. Papp, T. Biro, L. Kovacs, and L. Csernoch. 2002. Effect of protein kinase C on transmembrane calcium fluxes in HaCaT keratinocytes. *Exp. Dermatol.* 11:25–33.

Greenwood, I.A., and W.A. Large. 1998. Properties of a Cl^- current activated by cell swelling in rabbit portal vein vascular smooth muscle cells. *Am. J. Physiol.* 275:H1524–H1532.

Greenwood, I.A., J. Ledoux, and N. Leblanc. 2001. Differential regulation of Ca^{2+}-activated Cl^- currents in rabbit arterial and portal vein smooth muscle cells by Ca^{2+}-calmodulin-dependent kinase. *J. Physiol.* 534:395–408.

Hardie, R.C. 2003. Regulation of TRP channels via lipid second messengers. *Annu. Rev. Physiol.* 65:735–759.

Ishikawa, T., and D.I. Cook. 1993. A Ca^{2+}-activated Cl^- current in sheep parotid secretory cells. *J. Membr. Biol.* 135:261–271.

Jentsch, T.J., V. Stein, F. Weinreich, and A.A. Zdebik. 2002. Molecular structure and physiological function of chloride channels. *Physiol. Rev.* 82:503–568.

Jones, K.T., and G.R. Sharpe. 1994a. Ni^{2+} blocks the Ca^{2+} influx in human keratinocytes following a rise in extracellular Ca^{2+}. *Exp. Cell Res.* 212:409–413.

Jones, K.T., and G.R. Sharpe. 1994b. Thapsigargin raises intracellular free calcium levels in human keratinocytes and inhibits the coordinated expression of differentiation markers. *Exp. Cell Res.* 210:71–76.

Kansen, M., J. Keulemans, A.T. Hoogeveen, B. Scholte, A.B. Vaandrager, A.W. van der Kamp, M. Sinaasappel, A.G. Bot, H.R. de Jonge, and J. Bijman. 1992. Regulation of chloride transport in cultured normal and cystic fibrosis keratinocytes. *Biochim. Biophys. Acta.* 1139:49–56.

Koegel, H., and C. Alzheimer. 2001. Expression and biological significance of Ca^{2+}-activated ion channels in human keratinocytes. *FASEB J.* 15:145–154.

Koizumi, H., and A. Ohkawara. 1999. H_2 histamine receptor-mediated increase in intracellular Ca^{2+} in cultured human keratinocytes. *J. Dermatol. Sci.* 21:127–132.

Kuruma, A., and H.C. Hartzell. 2000. Bimodal control of a Ca^{2+}-activated Cl^- channel by different Ca^{2+} signals. *J. Gen. Physiol.* 115:59–80.

Lang, F., G.L. Busch, M. Ritter, H. Volkl, S. Waldegger, E. Gulbins, and D. Haussinger. 1998. Functional significance of cell volume regulatory mechanisms. *Physiol. Rev.* 78:247–306.

Lang, F., K. Klingel, C.A. Wagner, C. Stegen, S. Warntges, B. Friedrich, M. Lanzendorfer, J. Melzig, I. Moschen, S. Steuer, et al. 2000. Deranged transcriptional regulation of cell-volume-sensitive kinase hSGK in diabetic nephropathy. *Proc. Natl. Acad. Sci. USA.* 97:8157–8162.

Lemonnier, L., N. Prevarskaya, Y. Shuba, F. Vanden Abeele, B. Nilius, J. Mazurier, and R. Skryma. 2002a. Ca^{2+} modulation of volume-regulated anion channels: evidence for colocalization with store-operated channels. *FASEB J.* 16:222–224.

Lemonnier, L., Y. Vitko, Y.M. Shuba, F. Vanden Abeele, N. Prevarskaya, and R. Skryma. 2002b. Direct modulation of volume-regulated anion channels by Ca^{2+} chelating agents. *FEBS Lett.* 521: 152–156.

Mauro, T.M., R.R. Isseroff, R. Lasarow, and P.A. Pappone. 1993. Ion channels are linked to differentiation in keratinocytes. *J. Membr. Biol.* 132:201–209.

Nilius, B., and G. Droogmans. 2003. Amazing chloride channels: an overview. *Acta Physiol. Scand.* 177:119–147.

Nilius, B., M. Oike, I. Zahradnik, and G. Droogmans. 1994. Activation of a Cl^- current by hypotonic volume increase in human endothelial cells. *J. Gen. Physiol.* 103:787–805.

Nilius, B., J. Eggermont, T. Voets, and G. Droogmans. 1996. Volume-activated Cl^- channels. *Gen. Pharmacol.* 27:1131–1140.

Nilius, B., J. Prenen, T. Voets, K. Van den Bremt, J. Eggermont, and G. Droogmans. 1997. Kinetic and pharmacological properties of the calcium-activated chloride-current in macrovascular endothelial cells. *Cell Calcium.* 22:53–63.

Nilius, B., J. Prenen, U. Wissenbach, M. Bodding, and G. Droogmans. 2001. Differential activation of the volume-sensitive cation

channel TRP12 (OTRPC4) and volume-regulated anion currents in HEK-293 cells. *Pflugers Arch.* 443:227–233.

Pillai, S., and D.D. Bikle. 1992. Adenosine triphosphate stimulates phosphoinositide metabolism, mobilizes intracellular calcium, and inhibits terminal differentiation of human epidermal keratinocytes. *J. Clin. Invest.* 90:42–51.

Piper, A.S., I.A. Greenwood, and W.A. Large. 2002. Dual effect of blocking agents on Ca^{2+}-activated Cl^- currents in rabbit pulmonary artery smooth muscle cells. *J. Physiol.* 539:119–131.

Rosenbach, T., C. Liesegang, S. Binting, and B.M. Czarnetzki. 1993. Inositol phosphate formation and release of intracellular free calcium by bradykinin in HaCaT keratinocytes. *Arch. Dermatol. Res.* 285:393–396.

Rugolo, M., T. Mastrocola, M. De Luca, G. Romeo, and L.J. Galietta. 1992. A volume-sensitive chloride conductance revealed in cultured human keratinocytes by $36Cl^-$ efflux and whole-cell patch clamp recording. *Biochim. Biophys. Acta.* 1112:39–44.

Shen, M.R., G. Droogmans, J. Eggermont, T. Voets, J.C. Ellory, and B. Nilius. 2000. Differential expression of volume-regulated anion channels during cell cycle progression of human cervical cancer cells. *J. Physiol.* 529:385–394.

Shuba, Y.M., N. Prevarskaya, L. Lemonnier, F. Van Coppenolle, P.G. Kostyuk, B. Mauroy, and R. Skryma. 2000. Volume-regulated chloride conductance in the LNCaP human prostate cancer cell line. *Am. J. Physiol. Cell Physiol.* 279:C1144–C1154.

Venkatachalam, K., F. Zheng, and D.L. Gill. 2003. Regulation of canonical transient receptor potential (TRPC) channel function by diacylglycerol and protein kinase C. *J. Biol. Chem.* 278:29031–29040.

Voets, T., G. Droogmans, and B. Nilius. 1997. Modulation of voltage-dependent properties of a swelling-activated Cl^- current. *J. Gen. Physiol.* 110:313–325.

Voets, T., V. Manolopoulos, J. Eggermont, C. Ellory, G. Droogmans, and B. Nilius. 1998. Regulation of a swelling-activated chloride current in bovine endothelium by protein tyrosine phosphorylation and G proteins. *J. Physiol.* 506:341–352.

Wohlrab, D., and F. Markwardt. 1999. Influence of ion channel blockers on proliferation and free intracellular Ca^{2+} concentration of human keratinocytes. *Skin Pharmacol. Appl. Skin Physiol.* 12:257–265.

Wohlrab, D., J. Wohlrab, and F. Markwardt. 2000. Electrophysiological characterization of human keratinocytes using the patch-clamp technique. *Exp. Dermatol.* 9:219–223.

Yamamoto-Mizuma, S., G.X. Wang, L.L. Liu, K. Schegg, W.J. Hatton, D. Duan, T.L.B. Horowitz, F.S. Lamb, and J.R. Hume. 2004. Altered properties of volume-sensitive osmolyte and anion channels (VSOACs) and membrane protein expression in cardiac and smooth muscle myocytes from $Clcn3^{-/-}$ mice. *J. Physiol.* 557: 439–456.

Zhong, J., G.X. Wang, W.J. Hatton, I.A. Yamboliev, M.P. Walsh, and J.R. Hume. 2002. Regulation of volume-sensitive outwardly rectifying anion channels in pulmonary arterial smooth muscle cells by PKC. *Am. J. Physiol. Cell Physiol.* 283:C1627–C1636.